# Pb-doped CuO thin films synthetized by sol-gel method

**nassim touka** ( n.touka@univ-bouira.dz )
University of Bouira https://orcid.org/0000-0003-4101-4866
**D. TABLI**
University of Bouira
**N. TOUKA**
University of Bouira
**K. BADARI**
University of Bouira
**N. SELMI**
Nuclear Research Centre of Birine, Algeria.

**Research Article**

**Keywords:** CuO, Pb, Physical properties, Sol-gel, Thin films

**Posted Date:** March 15th, 2022

**DOI:** https://doi.org/10.21203/rs.3.rs-1435193/v1

# Pb-doped CuO thin films synthetized by sol-gel method

D. TABLI [1], N. TOUKA [1*], K. BADARI[1] and N. SELMI [2]

[1] Laboratory of Materials and Sustainable Development, Department of Physics, University of Bouira, Algeria.

[2] Nuclear Research Centre of Birine, Algeria.

**ABSTRACT**

*Sol-gel thin films of undoped CuO and Pb-doped CuO were deposited using the spin coating method. In three thin layers, the lead was introduced at two different concentrations (5 and 7%). The films produced were in the tenorite phase, with high purity and crystallinity, according to XRD structural characterization. The grain size of CuO films is affected by the Pb concentration and decreases as the Pb concentration increases, although the strain and dislocation density values increase as the Pb doping ratio increases. The structure of CuO was confirmed in all films by Raman and FTIR studies. In the presence of Pb dopants, SEM examinations revealed cubic and spherical nanostructured surfaces. With the value of the optical band gap increasing from 1.92 to 2.74 eV, there was a significant association between increasing Pb doping concentration and widening of the optical band gap.*

**Keywords:** CuO, Pb, Physical properties, Sol-gel, Thin films

## 1. INTRODUCTION

Copper oxide thin film semiconductors have received considerable attention in recent years because of their unique characteristics. They're commonly employed as an absorber material in solar cells [1-2] in gas sensors [3], biosensors [4], in catalysts [5] and as negative or positive electrode of lithium-ion batteries [6]. Cupric oxide (CuO) and cuprous oxide ($Cu_2O$), both oxidized copper oxides, are p-type semiconductors with optical direct band gaps of 1.3-3.7 eV and 1.8-2.5 eV, respectively [7-8]. Chemical vapor deposition [9], spray pyrolysis [10], thermal oxidation [11], pulsed laser deposition [12], electro-deposition [13], molecular beam epitaxy [14] and sol-gel [15]; were all utilized to synthesize copper oxide. Sol-gel technique, for example, has the benefit of forming high-purity, uniform, large-area thin films at a low temperature and at a low cost. Copper oxide film's physical properties are affected by doping, allowing them to be tailored for a range of applications. That many research projects on doped nanostructured films have previously been completed, there is still a demand for thin copper oxide films with attributes tailored to each application. In this work, we offer a simple and low-cost sol-gel spin coating approach for synthesizing and modifying the characteristics of copper oxide thin films. We opted to introduce lead (Pb) into the CuO lattice at two distinct concentrations (5 and 7%). The characteristics of the thin films produced were investigated as a function of Pb concentration.

## 2. MATERIAL AND METHODS

The precursors anhydrous copper (II) chloride ($CuCl_2$) (98%, Biochem) and anhydrous lead (II) acetate [$(CH_3COO)_2Pb$] (98%, Sigma Aldrich) were used as starting materials for the preparation of undoped and Pb doped CuO by the sol-gel method.

*n.touka@univ-bouira.dz

The details of the preparation of the undoped solution have been described elsewhere [16] except that in this work the quantity of the solvent methanol ($CH_3OH$) is 15 ml. Pb doping solution was prepared by dissolving lead (II) acetate anhydrous in undoped solution, we dissolve the necessary masses of this white powder in 15 ml to obtain the mass doping levels of 5% and 7%. The solution becomes homogeneous after stirring at 60 °C for 10 min.

The glass substrates were used to deposit thin films of CuO undoped and doped; these substrates are cleaned in an ultrasonic bath with acetone, ethanol, and deionized water before the deposition process starts. The technique used was spin coating. All of the films were deposited at room temperature, at a speed of 2800 rpm for 30 seconds. To remove organic contaminants, the films heated on a hot plate at 100 °C in air for 10 minutes after each spin-coating process. To make thin films of undoped CuO and Pb doped CuO with a three-layer thickness. Three times, the coating and drying process (one layer) was repeated. Finally, after the sample preparation is completed, they are all annealed in air for two hours at 350°C.

X-ray diffraction (XRD) was used to investigate the structural properties of the films using a PANalytical X'Pert PRO Diffractometer, scanning over 2θ of 25-60° with $CuK_\alpha$ irradiation ($CuK_\alpha$ = 1.5418 Å). A LabRAM HR Horiba Jobin Yvon spectrometer with a HeNe laser with a 632 nm excitation wavelength was used to record Raman spectra. Field emission scanning electron microscopy was used to examine the surface morphologies of the deposited films (JSM-7610F Plus). A Perkin Elmer Fourier transform infrared spectrometer was used to examine the vibrational bands of the produced thin films in the region of 4000–400 $cm^{-1}$. The optical absorption spectra were acquired in the wavelength range 300-800 nm using a Shimadzu UV-3101 PC UV-Vis-NIR spectrophotometer. At room temperature, all parameters were measured.

## 3. RESULTS AND DISCUSSION

### 3.1 Structural analysis

For two different Pb concentration of 5% and 7%, the characteristics of Pb doped CuO thin films have been examined. Figure 1 shows the effect of Pb on the structural characteristics of CuO thin films using XRD patterns. The observed peaks for undoped films at the positions 2θ = 31.77°, 35.60° and 38.75° were assigned to (-110), (002) and (111) crystallographic planes, respectively, for Pb doped CuO films we observe the disappearance of the peak located at 2θ = 31.77 ° and we note the appearance of a new peak located at 2θ = 49.15° assigned to (-202) crystallographic plane. According to JCPDS N° 00-045-0937, the XRD spectra of all samples revealed that they correspond to the space group C2/c of the monoclinic CuO structure with lattice parameters a = 4.6853 Å, b = 3.4257 Å, c = 5.1303 Å and = 99.5490°. It should be noted that the peak intensities and full width at half maximum (FWHM) change depending on the doping concentration. As a result, the $Pb^{2+}$ ions appear to replace the $Cu^{2+}$ ions in the CuO matrix without affecting the film's monoclinic structure. There are no peaks in the samples that relate to metallic Pb or its oxidation forms. The difference in the ionic radii of the host and the dopant atom creates a lattice strain [17] and leads to changes in the lattice parameters of the system when the dopant concentration increases because the ionic radius of the $Pb^{2+}$ dopant (1.2) is bigger than that of $Cu^{2+}$ (0.73). The presence of Pb ions in the CuO matrix is related with significant shifts in XRD patterns towards small angles [18]. The intensity of the (002) and (111) planes on the XRD spectra of the Pb doped CuO films significantly increases, indicating that the composite film's crystallinity has improved.

The structural parameters determined from the XRD patterns include grain size (D), FWHM (β), strain (ε), lattice spacing (d), and dislocation density (δ). According to Debye Scherer's formula [19], the average grain size value was calculated from the XRD peaks:

$$D = \frac{0{,}9\lambda}{\beta \cos\theta} \quad (1)$$

Where D is the crystallite size, λ = 1.5418 Å is the X-ray wavelength, β the FWHM of the peak, and θ is Bragg's angle.
The following equation was used to determine the strain values [20]:

$$\varepsilon = \frac{\beta}{4\tan(\theta)} \quad (2)$$

Bragg's equation was used to calculate the lattice spacing (d) values for all films:

$$2d\sin\theta = n\lambda \quad (3)$$

Where n is the order of diffraction, λ is the X-ray wavelength, and θ is the angle of diffraction.
The density of defects in CuO films which is the dislocation density (δ) was calculated using the equation:

$$\delta = \frac{1}{D^2} \quad (4)$$

where D is the crystallite size.

The lattice parameters were calculated using the monoclinic structure equation:

$$\frac{1}{d^2} = \frac{1}{(\sin\beta)^2}\left[\frac{h^2}{a^2} + \frac{k^2(\sin\beta)^2}{b^2} + \frac{l^2}{c^2} - \frac{2hl\cos\beta}{ac}\right] \quad (5)$$

where d is the inter-planer distance and h, k, and l are Miller indices for the particular Bragg reflection.

In this study we will use the (002) plane as a reference to compare the structural parameters of the undoped and Pb doped CuO thin films (Table 1) in order to facilitate the comparison. With increasing Pb content, the crystallite size was observed to decrease and the FWHM to increase. With increasing Pb concentration, the dislocation density in the crystal structure increased from $7.3922\times10^{-4}$ to $24.3624\times10^{-4}$.

The corresponding lattice spacing (d) reduced slightly in the presence of strain in the Pb doped CuO films and remained unchanged with the quantity of Pb doping. Because the strain increases with the increase in Pb concentration, the decrease in crystallite size can be considered to be associated with the increase in strain. Table 1 shows the estimated values of lattice parameters a, b, and c; these values agree with JPCDS card no. 00-045-0937.

Surface morphologies of undoped and Pb doped CuO thin film samples (5% and 7%) are shown in Figure 2, as a reminder; the samples were obtained by sequential deposition of three layers. In general, it can be seen that the surface of the films was greatly affected by the introduction of doping, especially for the grain size which was reduced compared to the pure CuO film. The films show an assemblage of granules that refer to films of a polycrystalline nature, and show a relatively dense surface structure consisting of crystals of spherical and cubic shapes of various sizes, which are coherently dispersed on the glass substrate. However, we observed islands

encapsulating nanometer-sized granules, and these islands become denser in the case of 7% doping ratio; therefore, the particles become less dense to form agglomerations of grain.

### 3.2 Raman analysis

For examining the phases of elaboration materials, Raman spectroscopy is a useful instrument. Because there are four atoms in the primitive cell, copper oxide possesses 12 phonon branches, three acoustic modes ($A_u + 2B_u$), six infrared active modes ($3A_u + 3B_u$), and three Raman active modes ($A_g + 2B_g$) [16]. Bands at Ag (296 $cm^{-1}$), Bg(1) (346 $cm^{-1}$), and Bg(2) (631 $cm^{-1}$) have been seen in pure CuO nanoparticles [16]. Figure 3 shows the room temperature Raman spectra of undoped CuO and Pb doped CuO thin films. Peaks at 294.5 $cm^{-1}$, 342.7 $cm^{-1}$, and 637 $cm^{-1}$ in the Raman spectra of CuO thin films correspond to Ag and the two Bg Raman active modes, respectively. Due to the obvious phonon confinement effect, the Raman spectra of Pb doped CuO films show shifts and broadening [21]. According to the XRD results, this behavior can be explained by a decrease in the size of the crystallites in the films of Pb doped CuO as the concentration of Pb increases.

### 3.3 FT-IR analysis

The FTIR spectra of undoped CuO and Pb doped CuO thin films are shown in Figure 4. Around 475 $cm^{-1}$, a broad metal-oxygen bond transmittance band was identified, which was attributed to Cu-O band vibrations [22], indicating the presence of CuO in the system. The appearance of a peak about 2363 $cm^{-1}$ due to the O =C= O vibrational band of $CO_2$ [23].

### 3.4 Optical analysis

The UV–Vis absorption spectra of samples are shown in Figure 5. In the visible region, the absorption intensity of the Pb doped thin film is higher than that of the undoped CuO thin film. The absorption properties of doped thin films were improved due to the increased defect sites. We used the Tauc formula [24] to determine the band gap energy $E_g$, we have plotted $(\alpha h\nu)^2$ versus $(h\nu)$,:

$$\alpha h\upsilon = C(h\upsilon - E_g)^{1/2} \quad (6)$$

where $\alpha$ is the optical absorption coefficient, $h\upsilon$ is the photon energy, $E_g$ is the optical band gap and C is the constant for a direct transition. Figure 6 shows how the band gap energies of the films were determined by extrapolating the linear part of the curves to the energy axis ($h\upsilon$). The optical band gap energies of undoped CuO and Pb doped CuO thin films were estimated to 1.92, 2.17 and 2.74 eV (Fig. 5) and found that $E_g$ increases with the Pb concentration. Because the size of the crystallites is reduced according to the results of the XRD, the optical band gap increases with the decrease of particle size.

## 4. CONCLUSION

The structural and optical characteristics of undoped CuO and Pb doped CuO thin films deposited on glass substrates using the sol-gel technique were studied. The CuO pure and Pb doped CuO composite films have a polycrystalline nature with a monoclinic structure, and the size of the crystals has reduced from 35.21 nm to approximately 19.36 nm, according to the structural analysis. SEM scans revealed that the concentration of Pb doping had an effect on the surface morphology of the Pb doped CuO composite. The Pb doped CuO thin films have a greater absorbance than the undoped CuO thin films. The optical band gap energies of undoped CuO and Pb doped CuO thin films were estimated at 1.92, 2.17 and 2.74 eV and found that $E_g$ increases

with the Pb concentration. This blue shift is due to the quantum confinement induced by the reduction in the size of the crystallites.

**REFERENCES**


[1] H. Chang, M. J. Kao, K. C. Cho, S.L. Chen, K.H. Chu, C.C. Chen, Curr. Appl. Phys.**11**, 19-22. (2011)

[2] L. Liu, K. Hong, X. Ge, M. Xu, J. Appl. Phys. A. **115**, 1147–1150 (2014)

[3] R. Li, J. Du, Y. Luan, Y. Xue, H. Zou, G. Zhuang, Z. Li, Sens. Actuators B. **65,** 156-164 (2012)

[4] K. Jindal, M. Tomar, V. Gupta, Biosens. Bioelectron. **38**, 11-18 (2012)

[5] S.M. Inamdar, V.K. More, S.K. Mandal, Tetrahedron Lett. **54**, 579-583 (2013)

[6] Z. Yin, Y. Ding, Q. Zheng, L. Guan, Electrochem. Commun. **20,** 40-43 (2012)

[7] A.Chen, H. Long, X. Li, Y. Li, G. Yang, P. Lu, Vacuum. **83**, 927-930 (2009)

[8] F. Gao, X.J. Liu, J.S. Zhang, M.Z. Song, N. Li, J. App. Phy. **111,** 084507 (2012)

[9] F .Bayansal, H.A. Çetinkara, S. Kahraman, H.M. Çakmak, H.S. Güder, Ceram Int. vol **38**, 1859-1866 (2012)

[10] V. Saravanan, P. Shankar, G.K. Mani, J.B.B. Rayappan, J. Anal. Appl. Pyrolysis. **111,** 272-277 (2015)

[11] M. Kaur, K.P. Muthe, S.K. Despande, S. Choudhury, J.B. Singh, N. Verma, S.K. Gupta, J.V. Yakhmi, J. Cryst. Growth. **289**, 670-675 (2006)

[12] M. Stamataki, D. Mylonas, D. Tsamakis, M. Kompitsas, P. Tsakiridis, E. Christoforou, Sens. Lett. vol **11**, 1964-1967 (2013)

[13] N.Mukherjee, B. Show, S.K. Maji, U. Madhu, S.K. Bhar, B.C. Mitra, G.G. Khan, A. Mondal, Mater. Lett. **65**, 3248-3250 (2011)

[14] K.P. Muthe, J.C. Vyas, S.N. Narang, D.K. Aswal, S.K. Gupta, D. Bhattacharya, R. Pinto, G.P. Kothiyal, S.C. Sabharwal, Thin Solid Films. **324**, 37-43 (1998).

[15] A.Y. Oral, E. Mensur, M.H. Aslan, E. Basaran, Mater. Chem. Phys. **83**, 140-144 (2004)

[16] N. Touka, D. Tabli, K. Badari, J. Optoelectron. Adv. M. **21**, 698-701 (2019)

[17] O. Mondal, M. Pal, R. Singh, D. Sen, S. Mazumder, M. Pal, J. Appl. Cryst. 48, 836-843 (2015)

[18] L.V. Devi, T. Selvalakshmi, S. Sellaiyan, A. Uedono, K. Sivaji, S. Sankar, J. Alloys Compd. **709**, 496-504 (2017).

[19] P. Scherrer, Göttinger Nachrichten Math. Phys. **2,** 98–100 (1918)

[20] S. Baturaya, A. Tombak, D. Batibaya, Y.S. Ocak, Appl. Surf. Sci. **477**, 91-95 (2017)

[21] J.F. Xu, W. Ji, Z.X. Shen, W.S. Li, S.H. Tang, X.R. Ye, D.Z. Jia, X.Q. Xin, J. Raman Spectrosc. **30**, 413-415 (1999)

[22] Y. Chang, “Fourier transform infrared (FTIR) analysis of copper oxide thin films prepared by metal organic chemical vapour deposition (MOCVD)”, MRS Online Proceedings Library, 443-448 (1992)

[23] J.D. Rodney, et al, Optik. **161**, 204-216 (2018)

[24] J. Tauc, “Amorphous & Liquid Semi-conductors”. Plenum Press, New York, NY (1974)

# Figures

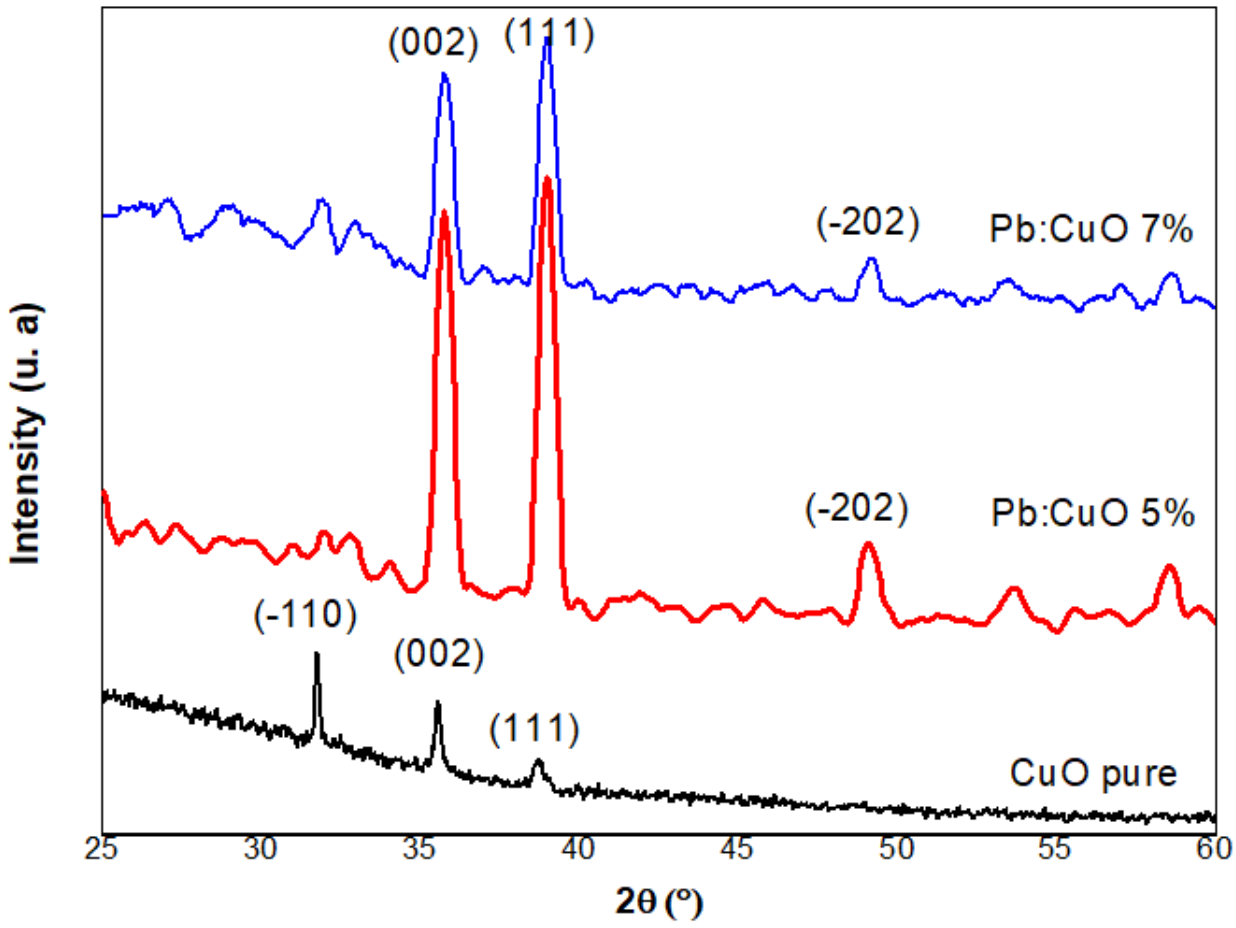


**Figure 1**

X-ray diffraction pattern of Pb doped CuO thin films for 5% and 7% Pb concentrations.

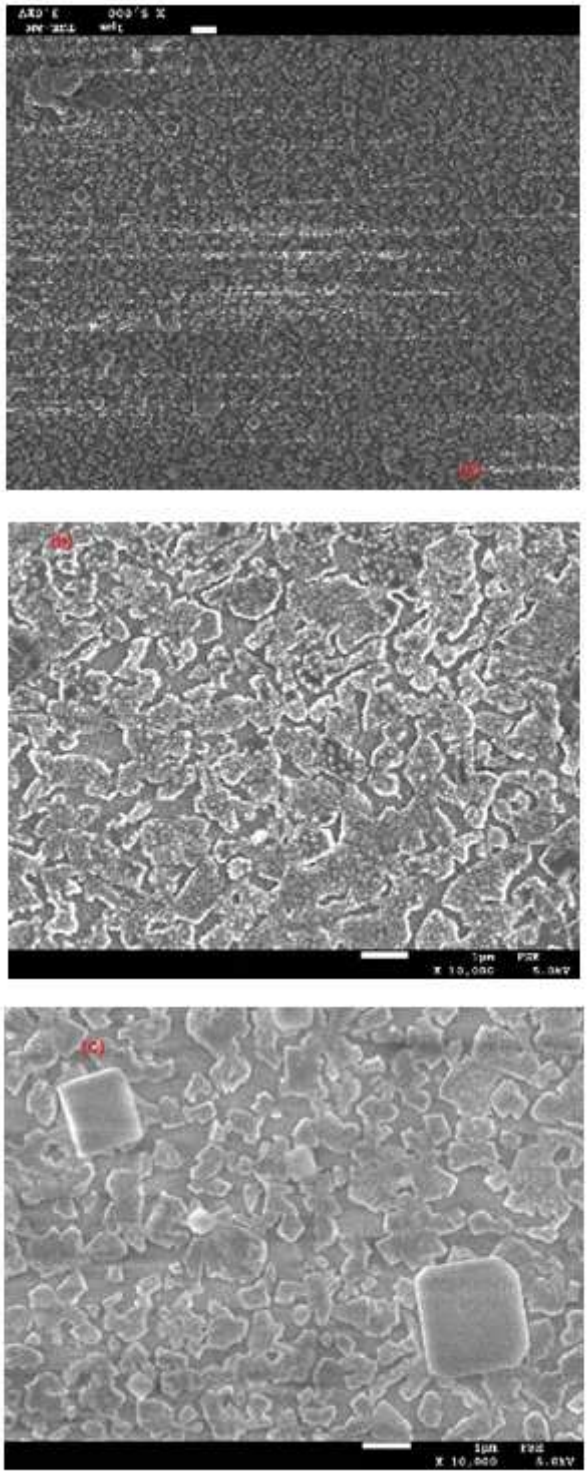

## Figure 2

SEM images of (a) undoped CuO thin film, (b) Pb doped CuO 5% and (c) Pb:CuO 7%.

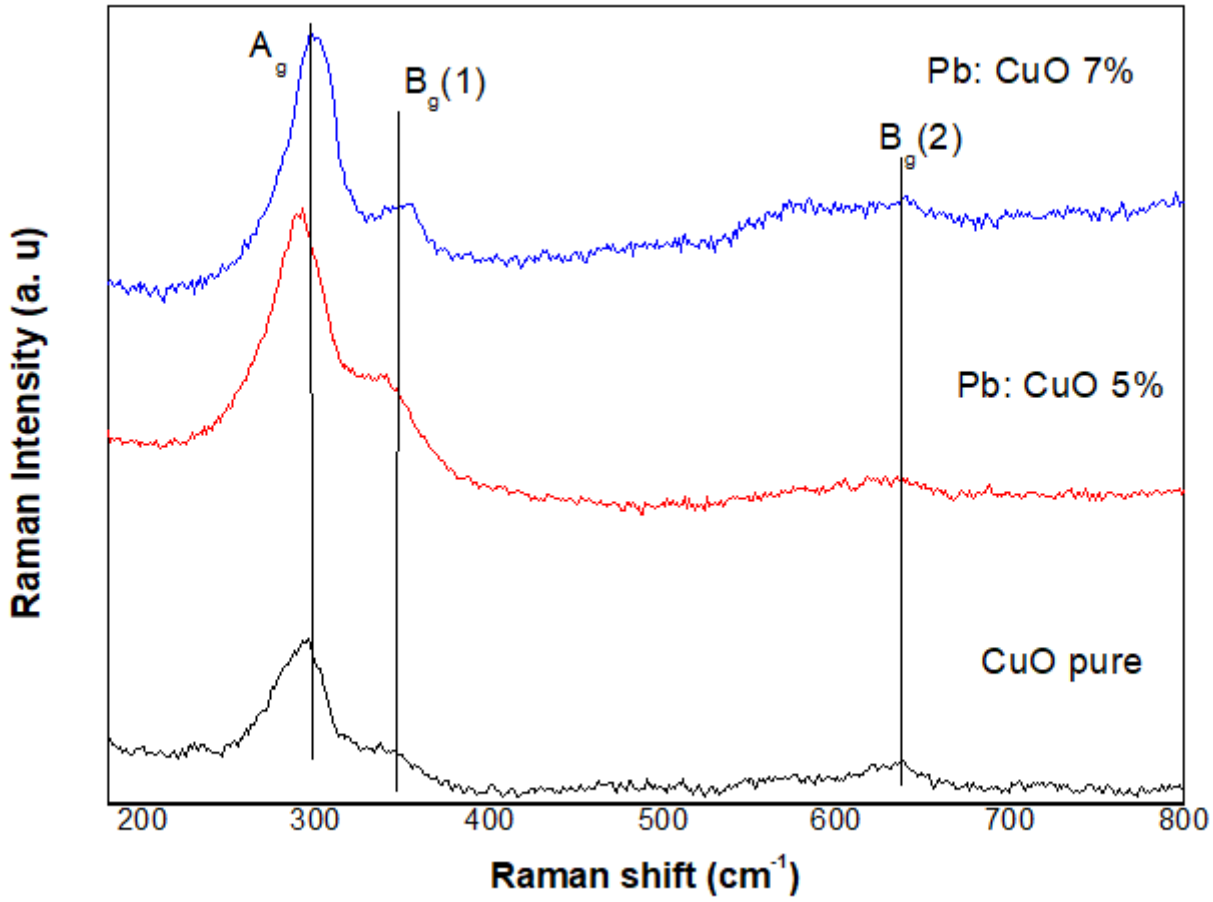


**Figure 3**

Raman spectra of undoped CuO and Pb doped CuO

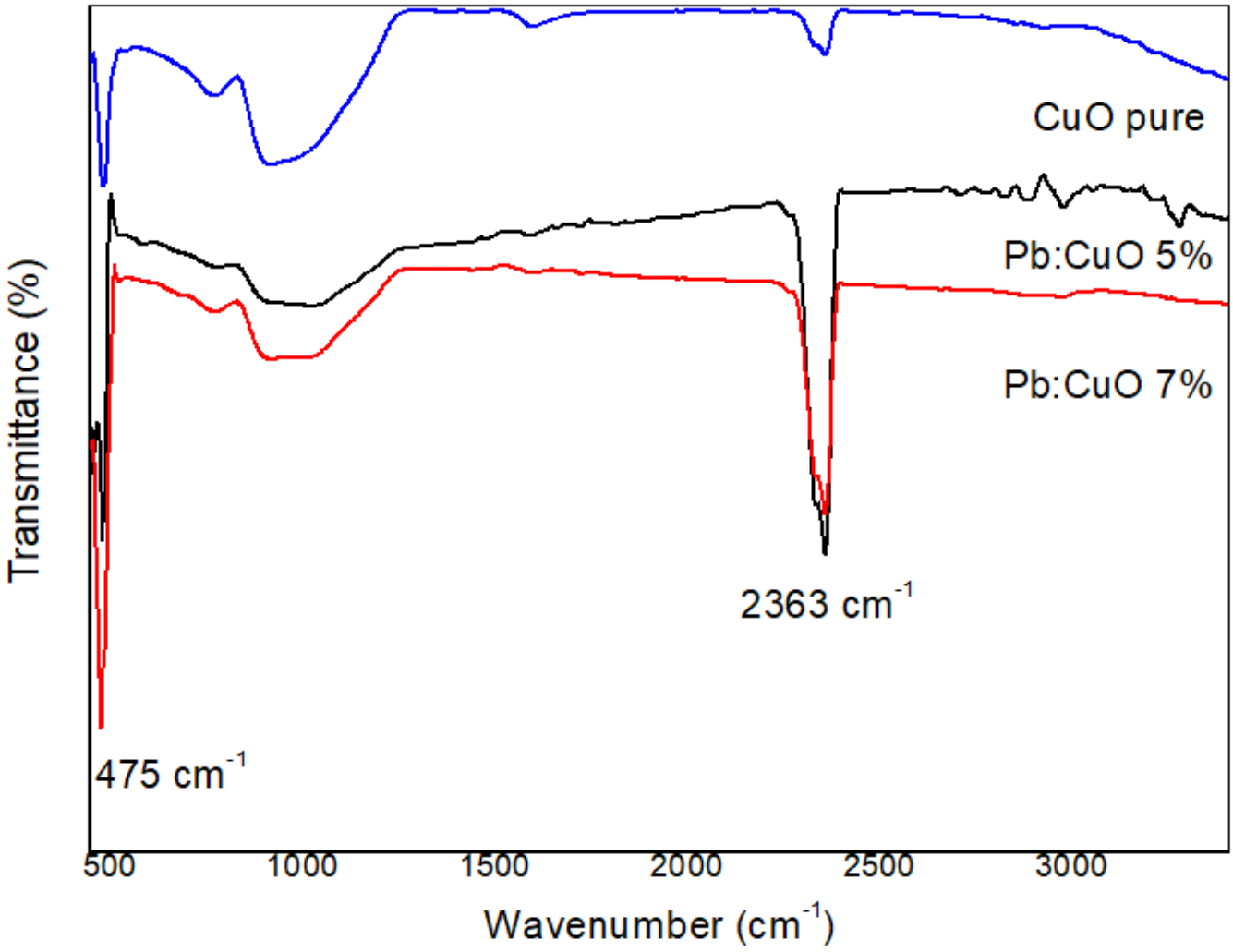


**Figure 4**

FTIR spectra of undoped CuO and Pb doped CuO

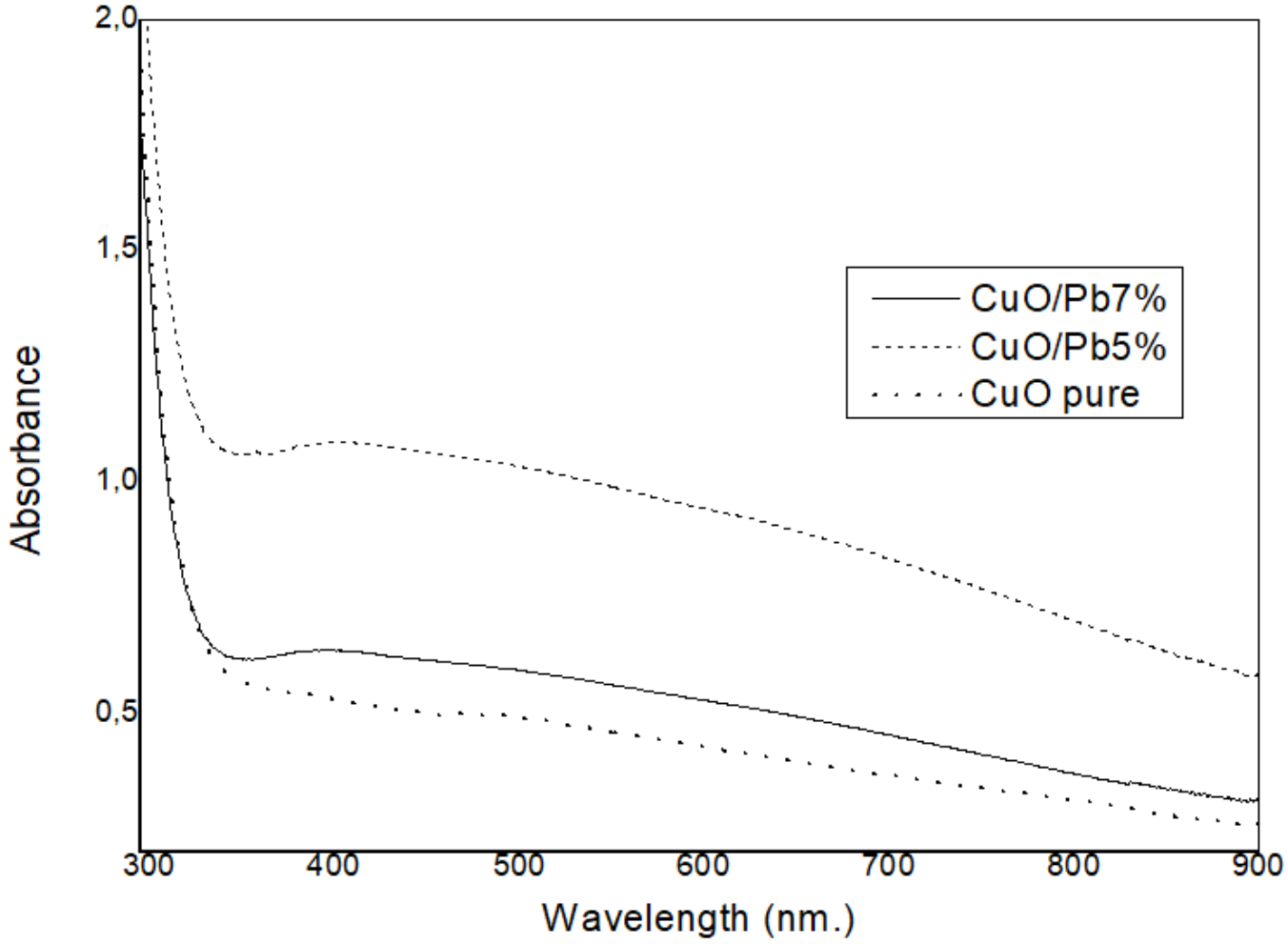


**Figure 5**

Optical absorption spectra of undoped CuO and Pb doped CuO thin films.

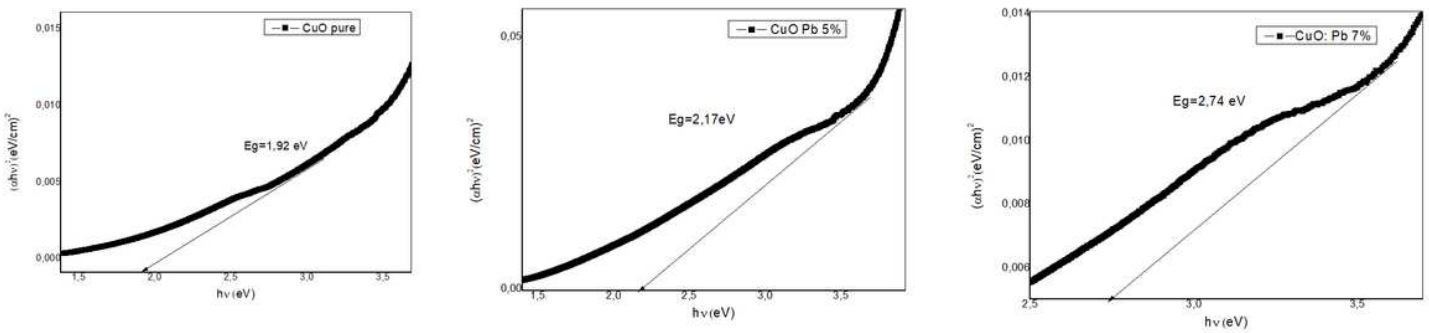


**Figure 6**

Band gap energy for undoped CuO and Pb doped CuO thin films.